

# *pp* Elastic Scattering at LHC in Near Forward Direction

M.M. ISLAM\* and R.J. LUDDY†

*Department of Physics, University of Connecticut, Storrs, CT 06269, USA*

\*islam@phys.uconn.edu †rjluddy@phys.uconn.edu

A.V. PROKUDIN

*Dipartimento di Fisica Teorica, Università Degli Studi di Torino, Via Pietro Giuria 1,*

*10125 Torino, Italy and Sezione INFN di Torino, Italy*

*Institute for High Energy Physics, 142281 Protvino, Russia*

prokudin@to.infn.it

## Abstract

We predict *pp* elastic differential cross section at LHC at the c.m. energy  $\sqrt{s} = 14$  TeV and momentum transfer range  $|t| = 0 - 10$  GeV<sup>2</sup>, which is planned to be measured by the TOTEM group. The field theory model underlying our phenomenological investigation describes the nucleon as a composite object with an outer cloud of quark-antiquark condensate, an inner core of topological baryonic charge, and a still smaller quark-bag of valence quarks. The model satisfactorily describes the asymptotic behavior of  $\sigma_{tot}(s)$  and  $\rho(s)$  as well as the measured  $\bar{p}p$  elastic  $d\sigma/dt$  at  $\sqrt{s} = 546$  GeV, 630 GeV, and 1.8 TeV. The large  $|t|$  elastic amplitude of the model incorporates the BFKL Pomeron in next to leading order approximation, the perturbative dimensional counting behavior, and the confinement of valence quarks in a small region within the nucleon.

PACS Nos.: 12.39.-x, 13.85.Dz, 14.20.Dh

Keywords: *pp* scattering; LHC/TOTEM; nucleon structure; hard Pomeron

*pp* elastic differential cross section at LHC in near forward direction at c.m. energy  $\sqrt{s} = 14$  TeV and momentum transfer  $|t| = 0 - 10$  GeV<sup>2</sup> is planned to be measured by the TOTEM (TOTal and Elastic Measurement) group [1]. Various models have been proposed to describe *pp* elastic scattering in the diffraction region  $|t| \simeq 0 - 0.5$  GeV<sup>2</sup>, such as: i) single Pomeron exchange with a trajectory  $\alpha_P(t) = 1.08 + 0.25t$  [2], ii) multiple Pomeron exchanges with single- and double-diffractive dissociation[3], iii) the incident proton viewed as made-up of two color dipoles in the target proton rest frame[4]. *pp* elastic  $d\sigma/dt$  at LHC all the way from  $|t| = 0$  to 10 GeV<sup>2</sup> has been predicted on the basis of three different models: a) impact-picture model [5] based on the Cheng-Wu calculation of QED tower diagrams [6], b) eikonalized Pomeron-Reggeon model using conventional Regge approach, but with multiple Pomeron-Reggeon exchanges included [7,8], c) effective field theory model that describes the nucleon as a chiral-bag with a quark-antiquark cloud [9,10]. A QCD motivated eikonalized model has also been proposed to predict *pp*  $d\sigma/dt$  at  $\sqrt{s} = 14$  TeV for  $|t| = 0 - 2.0$  GeV<sup>2</sup> [11]. This wide array of models attempting to describe *pp* elastic scattering at LHC reflects the view that quantitative understanding of this process will provide fundamental insight into the nonperturbative and the perturbative QCD dynamics.

The impact-picture model and the eikonalized Pomeron-Reggeon model predict besides the first dip-bump structure more diffraction-like secondary structures at large  $|t|$  [5, 7, 8]. The chiral-bag model with  $q\bar{q}$  condensate cloud, which we studied [9], predicts after the first dip-bump structure a smooth approximately exponential fall-off (known as Orear fall-off) and then a slower fall-off due to the transition from the nonperturbative regime to the perturbative regime. This change in the behavior of  $d\sigma/dt$  was shown only schematically in our previous work [9]. We have now been able to quantitatively address this question and study the predicted change of  $d\sigma/dt$ . Results of our investigation and the implications for the combined role of perturbative and nonperturbative QCD dynamics are briefly reported here.

We view *pp* elastic scattering in the perturbative regime as a hard collision of a valence quark from one proton with a valence quark from the other proton (Fig.1). The collision carries off

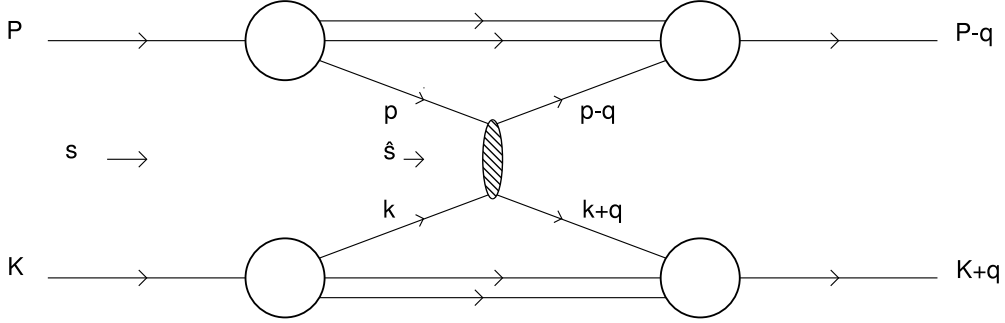


Figure 1: Hard collision of valence quarks from two different protons

the whole momentum transfer. This dynamical picture brings new features in our calculations: 1) Probability amplitude of a quark to have, say, momentum  $\vec{p}$  when the proton has momentum  $\vec{P}$  in the c.m. frame. 2) Quark-quark elastic amplitude at high energy and large momentum transfer, which is in the domain of perturbative QCD. The latter has been the focus of extensive studies following the original work of Balitsky, Fadin, Kuraev, and Lipatov (BFKL) [12]. The present status is that the  $qq$  elastic scattering occurs via Reggeized gluon ladders with rungs of gluons which represent gluon emissions in inelastic processes (BFKL Pomeron). It is a crossing-even amplitude which is a cut in the angular momentum plane with a fixed branch point at  $\alpha_{BFKL} = 1 + \omega$ . The value of  $\omega$  in the next-to-leading order (NLO) lies in the range 0.13-0.18 as argued by Brodsky et al.[13]. We refer to the BFKL Pomeron with next to leading order corrections included as the QCD “hard Pomeron”. In our investigation, we approximate this hard Pomeron by a fixed pole and take the  $qq$  scattering in Fig. 1 as

$$\hat{T}(\hat{s}, t) = i\gamma_{qq}\hat{s}(\hat{s} e^{-i\frac{\pi}{2}})^\omega \frac{1}{|t| + r_0^{-2}}, \quad (1)$$

where  $\hat{s} = (p + k)^2$ ,  $t = -\vec{q}^2$ . The phase in Eq.(1) follows from the requirement that  $\hat{T}(\hat{s}, t)$  is a crossing even amplitude. Eq.(1) represents the hard Pomeron amplitude in our calculations. If we want to describe just asymptotic  $qq$  scattering, we have to take into account unitarity corrections due to infinite exchanges of this Pomeron. This can be done by taking  $\hat{T}(\hat{s}, t)$  as the Born amplitude in an eikonal formulation [14], which leads to a black-disk description and requires  $\gamma_{qq} > 0$ . The radius of the black disk turns out to be  $R(\hat{s}) = r_0\omega \ln \hat{s}$ . Hence, the parameter  $r_0$  in Eq.(1) has the physical significance of a length scale that defines the black-disk radius of asymptotic quark-quark scattering.

We next examine how to obtain the  $pp$  elastic scattering amplitude from the process shown in Fig. 1. Let  $s$  be the square of the c.m. energy of the two colliding protons:  $s = (P + K)^2$ .  $\hat{s}$ , of course, is the square of the c.m. energy of the two colliding quarks. From Fig. 1, we see that initially we have a quark of momentum  $\vec{p}$ :  $|\vec{p}\rangle$  with a probability amplitude  $\varphi(\vec{p})$  in the c.m. frame in which the proton is moving with momentum  $\vec{P}$ . Similarly, we have a second quark with momentum  $\vec{k}$ :  $|\vec{k}\rangle$  with a probability amplitude  $\varphi(\vec{k})$  in the c.m. frame in which the other proton is moving with momentum  $\vec{K} = -\vec{P}$ . Thus, the initial state of the two colliding quarks is

$$|i\rangle = \varphi(\vec{p})|\vec{p}\rangle \varphi(\vec{k})|\vec{k}\rangle. \quad (2)$$

After the collision, we have a quark with momentum  $\vec{p} - \vec{q}$ :  $|\vec{p} - \vec{q}\rangle$  with a probability amplitude  $\varphi(\vec{p} - \vec{q})$ , and a quark with momentum  $\vec{k} + \vec{q}$ :  $|\vec{k} + \vec{q}\rangle$  with a probability amplitude  $\varphi(\vec{k} + \vec{q})$ . So,

the final state is

$$|f\rangle = \varphi(\vec{p} - \vec{q}) |\vec{p} - \vec{q}\rangle \varphi(\vec{k} + \vec{q}) |\vec{k} + \vec{q}\rangle. \quad (3)$$

The  $pp$  elastic scattering amplitude due to quark-quark scattering  $T_{qq}(s, -\vec{q}^2)$  from Fig. 1 is then

$$T_{qq}(s, -\vec{q}^2) = \sum_{\vec{p}} \sum_{\vec{k}} \varphi^*(\vec{p} - \vec{q}) \varphi^*(\vec{k} + \vec{q}) \langle \vec{k} + \vec{q} | \langle \vec{p} - \vec{q} | \hat{T}_{op} | \vec{p} \rangle | \vec{k} \rangle \varphi(\vec{p}) \varphi(\vec{k}), \quad (4)$$

where  $\langle \vec{k} + \vec{q} | \langle \vec{p} - \vec{q} | \hat{T}_{op} | \vec{p} \rangle | \vec{k} \rangle$  is the  $qq$  elastic scattering amplitude. Since this amplitude only depends on the invariants  $\hat{s} = (p + q)^2$  and  $\hat{t} = -\vec{q}^2$ , we can write

$$\langle \vec{k} + \vec{q} | \langle \vec{p} - \vec{q} | \hat{T}_{op} | \vec{p} \rangle | \vec{k} \rangle = \hat{T}(\hat{s}, -\vec{q}^2). \quad (5)$$

Eq.(4) then takes the form

$$T_{qq}(s, -\vec{q}^2) = \sum_{\vec{p}} \sum_{\vec{k}} \varphi^*(\vec{p} - \vec{q}) \varphi(\vec{p}) \hat{T}(\hat{s}, -\vec{q}^2) \varphi^*(\vec{k} + \vec{q}) \varphi(\vec{k}). \quad (6)$$

This equation makes it evident that  $\varphi^*(\vec{p} - \vec{q}) \varphi(\vec{p})$  and  $\varphi^*(\vec{k} + \vec{q}) \varphi(\vec{k})$  are the nonperturbative “impact factors” which modify the perturbative  $qq$  amplitude  $\hat{T}(\hat{s}, -\vec{q}^2)$ . The right-hand-side (RHS) of Eq.(6) needs to be multiplied by a factor of nine to take into account that there are three quarks in each proton[15]. We absorb this factor in the constant  $\gamma_{qq}$ .

To see the physical meaning of Eq.(6), let us assume that we can approximate  $qq$  scattering in Fig.1 by taking some average value of  $\hat{s} : \hat{s}_{av}$ . Of course,  $\hat{s}_{av}$  is going to be proportional to  $s$ . Eq.(6) then takes the form

$$T_{qq}(s, -\vec{q}^2) \simeq \sum_{\vec{p}} \varphi^*(\vec{p} - \vec{q}) \varphi(\vec{p}) \hat{T}(\hat{s}_{av}, -\vec{q}^2) \sum_{\vec{k}} \varphi^*(\vec{k} + \vec{q}) \varphi(\vec{k}), \quad (7)$$

which shows that the impact factors separate out. Each momentum sum in Eq.(7) can now be carried out and yields the form factor associated with the quark probability density in the c.m. frame. This probability density is Lorentz contracted, which means if  $\rho_0(\vec{r}')$  is the quark probability density at  $\vec{r}'$  in the proton rest frame and  $\rho(\vec{r})$  is the probability density at  $\vec{r}$  in the c.m. frame, then

$$\rho(\vec{b} + \vec{e}_3 z) = \gamma \rho_0(\vec{b} + \vec{e}_3 \gamma z), \quad (8)$$

where  $\gamma$  is the Lorentz contraction factor:  $\gamma = E/M = \sqrt{s}/(2M)$ ,  $\vec{r} = \vec{b} + \vec{e}_3 z$ , and  $\vec{e}_3$  is the unit vector in the direction of  $\vec{P}$ , i.e., the z-axis. If  $F(\vec{q})$  is the form factor associated with  $\rho_0(\vec{r})$ :

$$F(\vec{q}) = \int d^3 r e^{i\vec{q} \cdot \vec{r}} \rho_0(\vec{r}), \quad (9)$$

and  $\rho_0(\vec{r})$  is spherically symmetric, then

$$\begin{aligned} \sum_{\vec{p}} \varphi^*(\vec{p} - \vec{q}) \varphi(\vec{p}) &= \int d^3 r e^{-i\vec{q} \cdot \vec{r}} \rho(\vec{r}) \\ &= F(\vec{q}_\perp + \vec{e}_3 \frac{q_3}{\gamma}). \end{aligned} \quad (10)$$

In deriving Eq.(10), we have used  $\rho(\vec{r}) = \psi^*(\vec{r})\psi(\vec{r})$ , where the quark wave function  $\psi(\vec{r})$  is related to its momentum wave function  $\varphi(\vec{p})$  via the plane wave expansion:

$$\psi(\vec{r}) = \sum_{\vec{p}} \frac{e^{i\vec{p}\cdot\vec{r}}}{\sqrt{V}} \varphi(\vec{p}) \quad (11)$$

Eq.(7) now takes the form

$$T_{qq}(s, -\vec{q}^2) \simeq F(\vec{q}_\perp) \hat{T}(\hat{s}_{av}, -\vec{q}^2) F(\vec{q}_\perp), \quad \left( \frac{q_3}{\gamma} = \frac{2Mq_3}{\sqrt{s}} \rightarrow 0 \right). \quad (12)$$

The structure of Eq. (12) is easy to understand. It is the usual quantum-mechanical scattering amplitude of two composite objects described by the form factors and interacting via a basic process whose amplitude is  $\hat{T}(\hat{s}_{av}, -\vec{q}^2)$ . We take the form factor  $F(\vec{q})$  describing the quark probability density or number density in the nucleon rest frame to be a dipole:

$$F(\vec{q}) = \left( 1 + \frac{\vec{q}^2}{m_0^2} \right)^{-2}, \quad (13)$$

so that it satisfies the dimensional counting behavior  $t^{-2}$  for the form factor of a proton made up of three quarks [16,17,18].

Next we go back to Eq.(6) and no longer make the approximation of replacing  $\hat{s}$  by an average value. Inserting Eq.(1) in Eq.(6), we obtain

$$T_{qq}(s, -\vec{q}^2) = \sum_{\vec{p}} \sum_{\vec{k}} \varphi^*(\vec{p} - \vec{q}) \varphi(\vec{p}) i\gamma_{qq} \hat{s} (\hat{s} e^{-i\frac{\pi}{2}})^\omega \frac{1}{\vec{q}^2 + r_0^{-2}} \varphi^*(\vec{k} + \vec{q}) \varphi(\vec{k}). \quad (14)$$

Introducing light-cone variables  $P_+ = P_0 + P_3$ ,  $P_- = P_0 - P_3$ ,  $p_+ = p_0 + p_3$ ,  $p_- = p_0 - p_3$ , etc. and writing  $p_+ = x P_+$ ,  $k_- = x' K_-$ , we find  $\hat{s} \simeq x x' s$ , when  $P_+, K_- \rightarrow \infty$ . Eq.(14) then takes the separable form

$$T_{qq}(s, -\vec{q}^2) = \left( \sum_{\vec{p}} \varphi^*(\vec{p} - \vec{q}) \varphi(\vec{p}) x^{1+\omega} \right) i\gamma_{qq} s (s e^{-i\frac{\pi}{2}})^\omega \frac{1}{\vec{q}^2 + r_0^{-2}} \left( \sum_{\vec{k}} \varphi^*(\vec{k} + \vec{q}) \varphi(\vec{k}) x'^{1+\omega} \right). \quad (15)$$

In a frame where  $P_+ \rightarrow \infty$ ,

$$\sum_{\vec{p}} \varphi^*(\vec{p} - \vec{q}) \varphi(\vec{p}) x^{1+\omega} = \frac{M m_0^5}{8\pi} \int_0^1 dx \frac{x^{1+\omega}}{\left( \frac{m_0^2}{4} + M^2 x^2 \right)} I(q_\perp, \alpha(x)), \quad (16)$$

where

$$I(q_\perp, \alpha(x)) \equiv \int_0^\infty b db J_0(bq_\perp) \{bK_1[b\alpha]\}^2. \quad (17)$$

Here  $M$  is the nucleon mass,  $m_0$  is the mass parameter that occurs in the form factor Eq.(13),  $\alpha = \left( \frac{m_0^2}{4} + M^2 x^2 \right)^{\frac{1}{2}}$ , and  $\vec{q} \simeq \vec{q}_\perp$ . In deriving Eq. (16), we use momentum wave function  $\varphi(\vec{p})$  obtained from the Lorentz contracted probability density. It can be related to the rest frame wave function  $\varphi_0(\vec{p})$  in the following way:

$$\varphi(\vec{p}_\perp + \vec{e}_3 p_3) = \varphi_0(\vec{p}_\perp + \vec{e}_3 \frac{p_3}{\gamma}), \quad (18)$$

and yields the result

$$\varphi(\vec{p}_\perp + \vec{e}_3 p_3) = \left( \frac{2\pi m_0^5}{V_0} \right)^{\frac{1}{2}} \left( \frac{m_0^2}{4} + p_\perp^2 + \frac{p_3^2}{\gamma^2} \right)^{-2}. \quad (19)$$

( $V_0$  is the quantization volume in the rest frame.) The integral  $I(q_\perp, \alpha(x))$  can be evaluated analytically, and we obtain

$$I(q_\perp, \alpha(x)) = \frac{1}{8\alpha^4} \left\{ \frac{2}{a^3 a'} \ln(a' + a) + \frac{1}{a a'^3} \ln(a' + a) - \frac{1}{a^2 a'^2} - \frac{3a'}{a^5} \ln(a' + a) + \frac{3}{a^4} \right\}, \quad (20)$$

where  $a'^2 = \frac{q^2}{4\alpha^2}$ ,  $a^2 = a'^2 + 1$ . Let us denote by  $\mathcal{F}(q_\perp)$  the RHS of Eq.(16). Eq.(15) can then be expressed in the form

$$T_{qq}(s, -\vec{q}^2) = \mathcal{F}(q_\perp) i \gamma_{qq} s (s e^{-i\frac{\pi}{2}})^\omega \frac{1}{|t| + r_0^{-2}} \mathcal{F}(q_\perp). \quad (21)$$

For  $a'^2 = \frac{q^2}{4\alpha^2} \gg 1$  and  $a^2 \simeq a'^2$ , Eq.(20) yields

$$I(q_\perp, \alpha(x)) \simeq \frac{4}{q_\perp^4} \simeq \frac{4}{|t|^2}, \quad (|t| = \vec{q}^2 \simeq q_\perp^2). \quad (22)$$

Substituting this on the RHS of Eq.(16), we find

$$\mathcal{F}(q_\perp) \sim \frac{1}{|t|^2}. \quad (23)$$

Eq.(21) then leads to an amplitude

$$T_{qq}(s, -\vec{q}^2) \sim \frac{i \gamma_{qq} s (s e^{-i\frac{\pi}{2}})^\omega}{|t|^5}. \quad (24)$$

This results in differential cross section behavior for fixed  $s$  and large  $|t|$ :

$$\frac{d\sigma}{dt} \sim \frac{1}{|t|^{10}}, \quad (s \gg |t| \gg m_0^2 + 4M^2). \quad (25)$$

Eq.(25) shows that we obtain the behavior predicted by the perturbative QCD dimensional counting rules[16,17,18] for large  $|t|$ .

In our  $pp$  elastic scattering model, we now have two hard-collision amplitudes: one due to  $\omega$  exchange, the other due to the hard Pomeron exchange. Both collisions are accompanied by cloud-cloud diffraction scattering that reduces these amplitudes by an absorption factor  $\exp(i\hat{\chi}(s, 0))$  [19]. So the sum of the two hard amplitudes becomes

$$T_1(s, t) = e^{i\hat{\chi}(s, 0)} \left[ \pm \tilde{\gamma} s \frac{F^2(t)}{m^2 - t} + i \gamma_{qq} s (s e^{-i\frac{\pi}{2}})^\omega \frac{\mathcal{F}^2(q_\perp)}{|t| + r_0^{-2}} \right], (+\text{for } \bar{p}p, -\text{for } pp). \quad (26)$$

Using the same parameterization as before [9],

$$\tilde{\gamma} e^{i\hat{\chi}(s, 0)} = \hat{\gamma}_0 + \frac{\hat{\gamma}_1}{(s e^{-i\frac{\pi}{2}})^\hat{\sigma}}, \quad (27)$$

we find

$$T_1(s, t) = \left[ \hat{\gamma}_0 + \frac{\hat{\gamma}_1}{(s e^{-i\frac{\pi}{2}})^\hat{\sigma}} \right] \left[ \pm s \frac{F^2(t)}{m^2 - t} + i \tilde{\gamma}_{qq} s (s e^{-i\frac{\pi}{2}})^\omega \frac{\mathcal{F}^2(q_\perp)}{|t| + r_0^{-2}} \right], \quad (28)$$

where  $\tilde{\gamma}_{qq} = \gamma_{qq}/\tilde{\gamma}$ . The  $qq$  hard scattering term brings four new parameters: i)  $\tilde{\gamma}_{qq}$  which measures the relative strength of this term compared to the  $\omega$  exchange term; ii)  $\alpha_{BFKL} = 1+\omega$  which controls the high energy behavior; iii)  $r_0$  which provides the length scale for the black-disk radius of  $qq$  asymptotic scattering; iv)  $m_0$  which determines the quark wave function  $\psi_0(\vec{r}) = \sqrt{\rho_0(\vec{r})}$  and the size of the quark bag. Because of the different physical aspects associated with them, these four parameters form a minimal set.

We determine the parameters of the model by requiring that the model should describe satisfactorily the asymptotic behavior of  $\sigma_{tot}(s)$  and  $\rho(s)$  as well as the measured  $\bar{p}p$  elastic  $d\sigma/dt$  at  $\sqrt{s}=546$  GeV [20], 630 GeV [21], and 1.8 TeV [22, 23]. The results of this investigation are shown in Figs. 2 - 4 together with the experimental data. We obtain quite satisfactory descriptions. The dotted curves in Figs. 2 and 3 represent the error bands given by Cudell et. al. (COMPETE Collaboration) to their best fit [24]. We notice that our  $\sigma_{tot}(s)$  curve lies within their error band closer to the lower curve, but our  $\rho_{pp}(s)$  curve (dashed curve in Fig. 3) deviates from the band. As noted by Cudell et. al., such a deviation is not surprising – since a hard Pomeron occurs in our calculations and not in theirs. In fact, this hard Pomeron in conjunction with a crossing-odd absorptive correction [19] in our model leads to a crossing-odd amplitude (an odderon) and produces a visible difference between  $\rho_{\bar{p}p}(s)$  and  $\rho_{pp}(s)$  at large  $\sqrt{s}$ . The parameters describing the soft (small  $|t|$ ) diffraction amplitude and the hard (large  $|t|$ )  $\omega$ -exchange amplitude have been discussed before [9]. Their values are:  $R_0 = 2.77, R_1 = 0.0491, a_0 = 0.245, a_1 = 0.126, \eta_0 = 0.0844, c_0 = 0.00, \sigma = 2.70, \lambda_0 = 0.727, d_0 = 13.0, \alpha = 0.246, \hat{\gamma}_0 = 1.53, \hat{\gamma}_1 = 0.00, \hat{\sigma} = 1.46$  (the unit of energy is 1 GeV). The parameters  $\beta$  and  $m$  are kept fixed as previously:  $\beta=3.075, m=0.801$ . There are now seventeen adjustable parameters. The four new parameters describing the hard (large  $|t|$ )  $qq$  amplitude have the values  $\tilde{\gamma}_{qq} = 0.03, \omega = 0.15, r_0 = 2.00, m_0^2 = 12.0$ . (This value of  $m_0^2$  leads to a valence quark-bag of r.m.s. radius 0.2 F, while that of the baryonic charge core is 0.44 F.) These four parameters, however, cannot be determined reliably, because no large  $|t|$  elastic data are available in the TeV energy region.

Our prediction for  $pp$  elastic differential cross section at LHC at  $\sqrt{s}= 14$  TeV for the whole momentum transfer range  $|t| = 0 - 10$  GeV $^2$  is now given in Fig. 5 (solid curve). We obtain for  $\sigma_{tot}$  and  $\rho_{pp}$  the values 110 mb and 0.120 respectively. Also given in Fig. 5 are separate  $d\sigma/dt$  due to diffraction (dotted curve), due to hard  $\omega$ -exchange (dot-dashed curve), and due to hard  $qq$  scattering (dashed curve). As expected in our model, we find that in the small  $|t|$  region ( $|t| \simeq 0 - 0.5$  GeV $^2$ ) diffraction dominates, in the intermediate  $|t|$  region ( $|t| \simeq 1.0 - 4.0$  GeV $^2$ )  $\omega$ -exchange dominates, and in the large  $|t|$  region ( $|t| \gtrsim 6.0$  GeV $^2$ )  $qq$  scattering dominates. The three  $|t|$  regions correspond to cloud-cloud interaction, core-core scattering due to  $\omega$ -exchange, and valence  $qq$  scattering via QCD hard Pomeron. Therefore, they reflect the composite structure of the nucleon with an outer cloud, an inner core of topological baryonic charge, and a still smaller quark-bag of valence quarks.

We note that  $pp$  elastic differential cross section in the energy range  $\sqrt{s}= 27 - 62$  GeV and  $|t| \geq 3.5$  Gev $^2$  was observed to be approximately energy independent and falling off as  $t^{-8}$ . This was interpreted as due to the independent exchanges of three perturbative gluons [25, 26]. Later it was pointed out that the three gluons would Reggeize, so that color-octet exchanges would be suppressed. Instead, three color-singlet exchanges would take their place [27]. Eventually, as  $|t|$  increases, a single color-singlet exchange would dominate and lead to a  $t^{-10}$  fall-off as predicted by the perturbative QCD dimensional counting rules [16, 17, 18]. In our model, the dimensional counting behavior  $t^{-10}$  of  $d\sigma/dt$  originates from the hard  $qq$  amplitude in Eq. (28). This amplitude leads to a distinct change in the slope of the differential cross section from the intermediate  $|t|$  region to the large  $|t|$  region as seen in Fig. 5. For example, for  $1.0 \leq |t| \leq 3.0$  GeV $^2$ ,  $d\sigma/dt$  drops by more than two orders of magnitude, while for  $7.0 \leq |t| \leq 9.0$  GeV $^2$ ,  $d\sigma/dt$  drops by a factor of 4.2, i.e. less than an order of magnitude. Similar decrease in  $d\sigma/dt$  slope was observed

at ISR by De Kerret et.al. for  $|t| \gtrsim 6.5 \text{ GeV}^2$  at a much lower energy:  $\sqrt{s} = 53 \text{ GeV}$  [28]. Lepage and Brodsky[18], however, pointed out that at such low energies it would be hard to distinguish between amplitudes that lead to  $t^{-8}$  and  $t^{-10}$  asymptotic behavior.

We conclude that, if precise measurement by the TOTEM group corroborates our predicted slow fall-off of  $pp$  elastic  $d\sigma/dt$  in the large  $|t|$  region, then that will provide evidence for the hard  $qq$  amplitude occurring in Eq. (28). This, in turn, will imply: i) presence of the QCD hard Pomeron, ii) perturbative QCD dimensional counting behavior at asymptotic  $|t| (>> 10 \text{ GeV}^2)$ , and iii) the confinement of valence quarks in a small region within the proton.

Much of this work was done when one of us (MMI) was at the Yang Institute for Theoretical Physics at SUNY Stony Brook on sabbatical leave. He wishes to thank George Sterman, Director of the Institute, and other colleagues there for their hospitality. He also wishes to thank Michael Rijssenbeek and George Sterman for stimulating discussions.

## References

1. TOTEM: Technical Design Report, Jan. 2004 (CERN-LHCC-2004-002).
2. A. Donnachie, H.G. Dosch, P.V. Landshoff, and O. Nachtmann, *Pomeron Physics and QCD*, Cambridge University Press (2002).
3. V. A. Khoze, A. D. Martin, and M.G. Ryskin, *Eur. Phys.J C18* (2000) 167.
4. J. Bartels, E. Gotsman, E. Levin, M. Lublinsky, and U. Maor, *Phys Lett.B* 556 (2003) 114.
5. C. Bourrely, J. Soffer, and T.T. Wu, *Eur. Phys.J C28* (2003) 97.
6. H.Cheng and T.T.Wu, *Expanding Protons: Scattering at High Energies*, MIT Press, Cambridge, MA (1987).
7. P. Desgrolard, M. Giffon, E. Matynov, and E. Predazzi, *Eur. Phys.J C16* (2000) 499.
8. V. A. Petrov and A.V. Prokudin, *Eur. Phys.J C23* (2002) 135.
9. M. M. Islam, R. J. Luddy, and A.V. Prokudin, *Mod. Phys. Lett.A* 18 (2003) 743.
10. M. M. Islam, R. J. Luddy, and A.V. Prokudin, in *AIP Conference Proceedings Vol.698, 2003 (Intersections of Particle and Nuclear Physics, edited by Z. Parsa)* p.142. [hep-ph/0307355]
11. M.M. Block, E.M. Gregores, F. Halzen and G. Pancheri, *Phys.Rev. D60*, (1999) 054024.
12. J. R. Forshaw and D. A. Ross, *Quantum Chromodynamics and the Pomeron*, Cambridge University Press (1997).
13. S. J. Brodsky, V. S. Fadin, V.T. Kim, L. N. Lipatov, and G. B. Pivovarov, *JETP Lett.* 70 (1999) 155.
14. A. B. Kaidalov, *Regge Poles in QCD* in *Handbook of QCD*, Vol.1, edited by M. Shifman and B. Ioffe (World Scientific, 2001) p. 603.
15. The quarks in our field theory model (Ref. 10) are massless effective color-singlet quarks and not the QCD current quarks.
16. V. A. Matveev, R. M. Muradian, and A. N. Tavkhelidze, *Lett.Nuovo Cimento* 7 (1973) 719.
17. S. J. Brodsky and G. R. Farrar, *Phys.Rev.Lett.* 31 (1973) 1153; *Phys.Rev.D* 11 (1975) 1309.
18. G.P. Lepage and S.J. Brodsky, *Phys.Rev.D* 22 (1980) 2157.
19. M.M. Islam, B. Innocente, T. Fearnley, and G. Sanguinetti, *Europhys. Lett.* 4 (1987) 189.
20. M. Bozzo et.al., UA4 Collaboration, *Phys.Lett. B147* (1984) 385; *B155*, (1985) 197.
21. D. Bernard et.al. *Phys.Lett. B171* (1986) 142.
22. N. Amos et.al., *Phys.Lett. B247* (1990) 127.
23. F. Abe et.al., *Phys.Rev. D50* (1994) 5518.
24. J.R. Cudell et.al., *Phys.Rev.Lett.* 89 (2002) 201801.
25. A. Donnachie and P.V. Landshoff, *Z. Phys. C* 2(1979)55.
26. A. Donnachie and P.V. Landshoff, *Phys. Lett. B* 387(1996) 637.
27. M. G. Sotiropoulos and G. Sterman, *Nucl.Phys. B* 425 (1994) 489.
28. H. De Kerret et al., *Phys. Lett. B* 68(1977) 374.

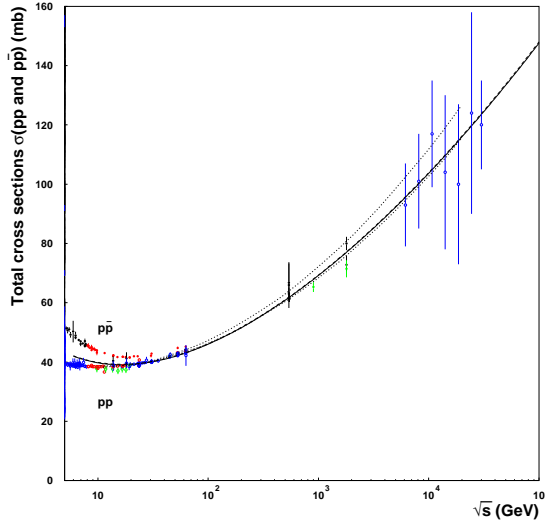


Figure 2: Solid curve represents our calculated total cross section as a function of  $\sqrt{s}$ . Dotted curves represent the error band given by Cudell et al. [24].

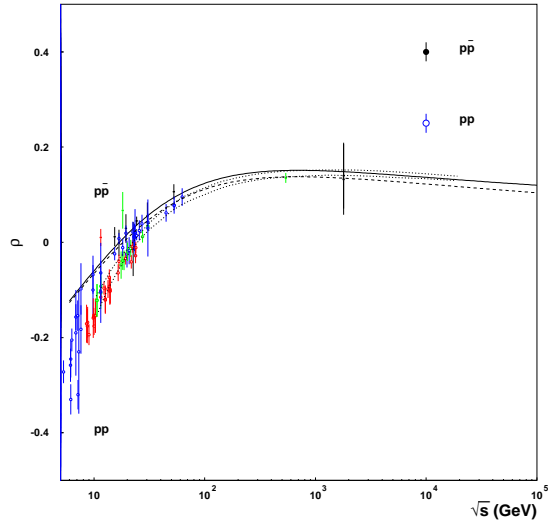


Figure 3: Solid and dashed curves represent our calculated  $\rho_{\bar{p}p}$  and  $\rho_{pp}$  as functions of  $\sqrt{s}$ . Dotted curves represent the error band given by Cudell et al. [24].

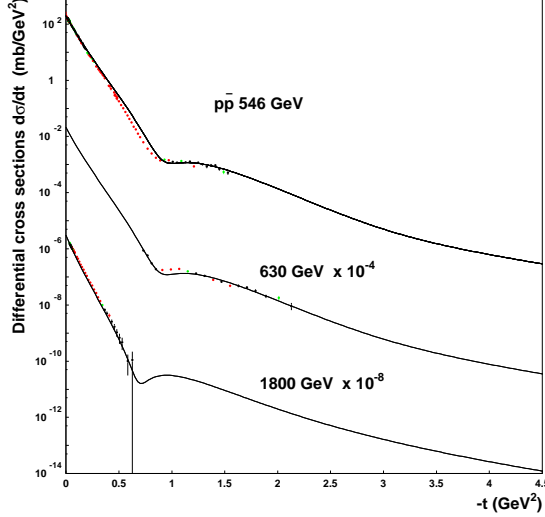


Figure 4: Solid curves show our calculated  $d\sigma/dt$  at  $\sqrt{s} = 546, 630$  and  $1800$  GeV. Experimental data are from references [20], [21] and [22, 23].

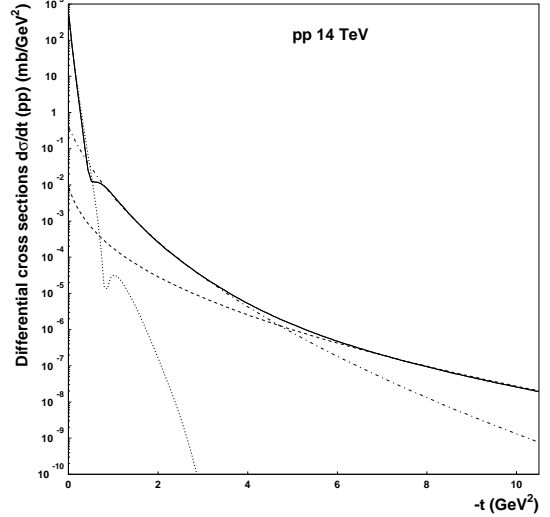


Figure 5: Solid curve shows our predicted  $d\sigma/dt$  for pp elastic scattering at  $\sqrt{s} = 14$  TeV at LHC. Dotted curve represents  $d\sigma/dt$  due to diffraction only. Similarly, dot-dashed curve and dashed curve represent  $d\sigma/dt$  due to hard  $\omega$ -exchange and hard  $qq$  scattering only.